Electric Power Systems Research 220 (2023) 109280

Contents lists available at ScienceDirect

Electric Power Systems Research

journal homepage: www.elsevier.com/locate/epsr

Moving average-based mitigation of exponentially decaying DC components

T.S. Menezes [a,*], R.A.S. Fernandes [b], D.V. Coury [a]

[a] Department of Electrical and Computer Engineering, São Carlos School of Engineering, University of São Paulo, São Carlos 13566-590, Brazil
[b] Department of Electrical Engineering, Federal University of São Carlos, São Carlos 13565-905, Brazil

ARTICLE INFO

Keywords:
DC component
Discrete Fourier Transform
Moving average filter
Phasor estimation

ABSTRACT

Exponentially decaying DC components are normally found in current signals during a fault in an electric power system. As these components generally decrease the precision of phasor estimation techniques, they must be filtered out. Thus, this paper proposes an alternative approach to mitigate exponentially decaying DC components. Firstly, the damping factor of the input signal is estimated using its moving average. Then, based on the symmetry of the sinusoidal signal, the value of the exponentially decaying DC component is calculated and subtracted. Tests were conducted with simulated signals, comparing the proposed approach with the state-of-the-art literature. Additionally, all the techniques were embedded in a microcontroller to validate their performances in hardware. Overall, the proposed approach presented the best software performance, compatible with hardware embedded applications in a low-cost microcontroller, proving to be an effective methodology to mitigate the DC offset.

1. Introduction

Eletrical signals in power systems are susceptible to different sources of unwanted distortions, such as noise, harmonics, and DC offset. Due to the resistor-inductor (RL) circuit of the power lines, a fault creates time variant DC offsets that follows an exponentially decay behavior. Thus, the phasor estimation of the fundamental component of the signals might be degraded by its presence. For this reason, the Exponentially Decaying DC (EDDC) component must be eliminated or, at least, mitigated.

Some early propositions to mitigate the EDDC component were the cosine filter for the Discrete Fourier Transform (DFT) [1], and the digital mimic filter [2]. Later, some approaches were proposed to improve the DFT performance. In [3], the authors proposed a phasor estimation algorithm that is immune to the DC component. Firstly, it uses the half-cycle Walsh transform to compute the DC component. Then, the phasor estimation is performed by a half-cycle DFT. Afterwards, if the estimated DC component exceeds a pre-defined threshold, the phasor estimation will be compensated. There are other similar propositions, such as the modified cosine filter [4], three different sine and cosine filters [5], interactive compensation of real and imaginary components [6], and an improved DFT using even and odd sample compensation [7]. Although these approaches perform well, they cannot be further improved by using a more recent and/or robust phasor estimation technique.

Additionally, there were some studies utilizing different approaches to mitigate the EDDC component based on the signal integration [8–10], Hilbert transform [11,12], second-order derivative [13], artificial neural networks [14,15], eigenvalues [16], empirical Wavelet transform [17], complex frequency filter [18], digital finite impulse response filter [19], non-linear least square method [20], intrinsic time-scale decomposition [21], re-sampling [22], sub-cycle samples [23], mathematical morphology [24], least square method using adaptive coefficients [25], and signal periodicity [26]. Some of the above-mentioned approaches, which are filtering techniques to mitigate the EDDC component, will be further detailed in Section 2, due to their similarities with the proposed approach.

From the previously presented context, this paper proposes an alternative EDDC component filter. The proposed approach uses the symmetry and moving average of the signal to mitigate the EDDC component. Firstly, the moving average is applied over the last cycle to calculate the damping factor (τ). Then, using the periodicity and symmetry of the signal, the EDDC is estimated and subtracted from the original signal, thus filtering it. After these procedures, the resulting signal can be processed by any phasor estimation method, such as the DFT. Thus, the approaches presented in Section 2 were compared using simulated fault current signals with EDDC, harmonics, and noise. Additionally, all the approaches were embedded in hardware to evaluate their performance and applicability in a real implementation with external factors, such as noise and digitization errors. Therefore, the

* Corresponding author.
E-mail address: thiagosm@usp.br (T.S. Menezes).

https://doi.org/10.1016/j.epsr.2023.109280
Received 1 December 2022; Received in revised form 9 February 2023; Accepted 4 March 2023
Available online 11 March 2023

present paper contributes to advancing the state-of-the-art in terms of: (i) validating the approach in hardware; (ii) evaluating the proposed approach with real harmonic profiles, frequency variation, different noise levels and sample rates; and (iii) an extensive comparison with other approaches using numerical indices.

The following sections are organized as follows. Section 2 presents the related studies used for the sake of comparison with the proposed approach. Next, Section 3 describes the formulation of the proposed approach. Section 4 presents the results and analysis for different scenarios, including tests in hardware. Finally, the conclusions are drawn in Section 5.

2. Related studies

As mentioned before, some related filtering approaches have similarities with the proposed one to mitigate the EDDC component. These approaches are described next and used in a comparative analysis.

The first approach is the digital mimic filter proposed by [2], which is widely known in the literature. This approach mimics an RL circuit to filter the EDDC component. Although the mimic filter was easily implemented and had a low computational burden, it needed to be adjusted to a specific damping factor. Nevertheless, it performed as a high-pass filter, which could amplify high-frequency components in the input signal, such as noise.

As filters based on numerical integration were addressed by different papers in the literature, the approach proposed in [8] was also investigated. The authors used the numerical integration of the input signal to estimate the damping factor of the EDDC component. Although the approach presented some promising results, analysis were performed by visual inspection, utilizing only a few cases.

A different technique to mitigate the EDDC component was proposed by [13]. This technique used the second-order derivative to estimate the EDDC, considering that the reactance of the line is greater than the resistive component. The authors evaluated the approach using synthetic and simulated signals, resulting in a fast convergence overall. However, the results did not include analysis in the presence of noise, which would result in numerical divergence and high errors due to the second-order derivative.

Xiong et al. [26] presented a more recent approach. The approach used the periodicity and symmetry of the input signal to estimate the EDDC component. The tests included experimental validation, but the result was shown graphically as an oscilloscope waveform only for a single case.

In summary, some aspects of the aforementioned studies should be highlighted. First of all, none of them evaluated their proposition considering noisy measurements, which appear in real applications. Additionally, despite the importance of a hardware embedded analysis, only the authors of [26] conducted experimental evaluations. Finally, although some studies perform tests considering the presence of harmonics, a very specific harmonic content was inserted into the signal. Therefore, in the present paper, the proposed approach for mitigating the EDDC component was extensively evaluated and compared with the other techniques. The tests considered simulated signals with real harmonic profiles, different noise levels, and different sample rates. Furthermore, the proposed approach was embedded in hardware to validate the applicability of the proposition. All the scenarios were evaluated with numerical indices to quantify the performance of each of the approaches analyzed.

3. The proposed methodology

In order to illustrate the proposed approach, an input signal $x(t)$ consisting of an EDDC with magnitude A_0, damping factor τ, and fundamental sinusoidal component with magnitude A_1 must be considered, expressed as:

$$x(t) = A_0 e^{-t/\tau} + A_1 cos(\omega t + \phi). \tag{1}$$

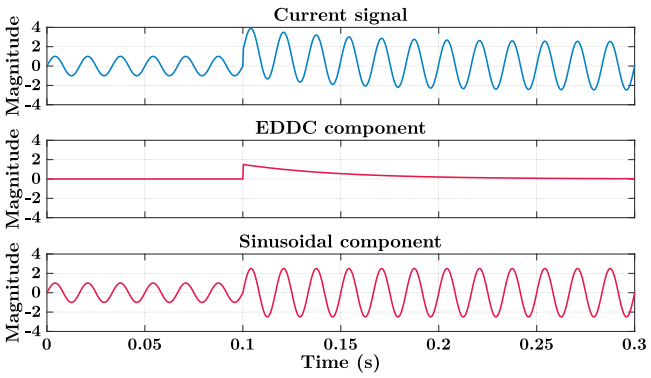

Fig. 1. Example of a current signal with its EDDC and sinusoidal components.

This input signal with EDDC and sinusoidal components can be graphically presented as shown in Fig. 1.

As the second term of (1) is purely sinusoidal, its average value is equal to zero. Thus, the moving average of a full cycle at a given instant t ($ma(t)$) of the input signal will be an approximation of the EDDC component, as shown in (2):

$$ma(t) \approx A_0 e^{-t/\tau}. \tag{2}$$

Additionally, the second term of (1) is also periodic, therefore its moving average at the previous sample ($ma(t-\Delta t)$) can be approximated to:

$$ma(t-\Delta t) \approx A_0 e^{-(t-\Delta t)/\tau} = A_0 e^{-t/\tau} \cdot e^{\Delta t/\tau}. \tag{3}$$

Dividing (2) by (3), the damping factor τ can be isolated and estimated as:

$$\tau \approx \frac{-\Delta t}{ln\left(\frac{ma(t)}{ma(t-\Delta t)}\right)}. \tag{4}$$

Some constraints must be defined to ensure the numerical convergence of the damping factor estimation. Firstly, to prevent the value of the natural logarithm from reaching minus infinite or leading to a division by zero, neither the current or the past moving average should be equal to zero. Secondly, the ratio between both moving averages will be close to one at a steady-state behavior. As a result, the natural logarithm tends towards zero, and the value of τ tends towards positive infinite. Therefore, both moving averages cannot have the same value. Under these two constraints, the damping factor holds its previous value. Otherwise, the damping factor is updated using (4). All the constraints are summarized in (5):

$$\tau(t) = \begin{cases} \tau(t-1) & \text{, if } ma(t)\cdot ma(t-\Delta t) \le 0 \\ & \text{or } ma(t) = ma(t-\Delta t) \\ \frac{-\Delta t}{ln\left(\frac{ma(t)}{ma(t-\Delta t)}\right)} & \text{, otherwise.} \end{cases} \tag{5}$$

Then, considering that the input signal is sinusoidal and periodical (since each window represents a cycle), the sum of the current sample ($x(t)$) and the sample at the last half cycle ($x(t-T/2)$) will be zero. Thus, the sinusoidal component will be canceled, resulting in:

$$\begin{aligned} x(t) + x(t-T/2) &= A_0 e^{-t/\tau} + A_0 e^{-t/\tau} \cdot e^{(T/2)/\tau} \\ &= A_0 e^{-t/\tau}(1 + e^{(T/2)/\tau}). \end{aligned} \tag{6}$$

Replacing the damping factor (τ) previously estimated by (4) in (6), the value of the EDDC component can be determined as:

$$A_0 e^{-t/\tau} = \frac{x(t) + x(t-T/2)}{(1 + e^{(T/2)/\tau})}. \tag{7}$$

To improve the execution speed of the proposed algorithm, a more computationally efficient approach was used to calculate the moving average. This fast-moving average algorithm has the same precision,

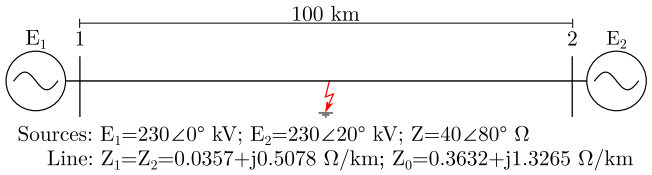

Fig. 2. Test system and its electrical parameters.

but it requires less computational resources to run it. For the first iteration (when $k = 1$), the moving average is computed as shown in (8):

$$ma_k = \frac{1}{N}\sum_{j=1}^{N} x_{k+j}, \tag{8}$$

where N represents the signal length.

For all subsequent iterations, the moving average updates its previous value by adding the new sample and subtracting the oldest one. It is worth noting that this fast-moving average algorithm has a constant computational burden, regardless of the signal length. The fast-moving average calculation is presented in (9):

$$ma_k = ma_{k-1} + \frac{1}{N}\left(x_k - x_{k-N}\right). \tag{9}$$

Based on this methodology, some scenarios were considered to test the performance of the proposed approach, as presented in the next section. All the results presented in the paper used the fast-moving average algorithm.

4. Results and analysis

The evaluation of the proposed approach was performed using a transmission system modeled on the software ATP (Alternative Transients Program). This is a 60 Hz, 230 kV system with a 100 km transmission line connecting the two sources, as presented in [13]. The system and its electrical parameters are illustrated in Fig. 2.

The fault currents were generated for single-phase faults (phase A to ground), varying their locations (from 1 km up to 90 km from bus 1 in increments of 10 km), fault resistances (from 0 Ω up to 20 Ω in increments of 2 Ω), and fault inception angles (from 0° up to 355° in increments of 5°). This combination resulted in a total of 7920 faults. All the currents were measured at bus 1, in which the fault started at 0.5 s, and had a total simulation time of 2 s.

In order to compare the performance of the proposed method, as previously mentioned, other filtering techniques in the literature were implemented [2,8,13,26]. It must be observed that none of the approaches implemented require parameterization, except the digital mimic filter, which was set to a time constant equal to two cycles. This is the same value used in the original paper [2].

4.1. Evaluation indices

The output of the different approaches was evaluated based on the indices proposed by [2]. These indices needed a reference value for the phasor at steady-state (X_{ref}). This reference value was calculated as the average peak value of the last 15 cycles of the simulated signal, when the EDDC component was negligible. Then, all the current signals were normalized to have a steady-state magnitude of 1 pu after the fault.

The first performance index (PI_1) evaluates the steady-state oscillations. It is defined as the sum of phasor absolute errors from the first time the estimated phasor (X) reaches its steady-state value (t_0) until the end of the simulation (t_{end}), as shown in (10):

$$PI_1 = \sum_{k=t_0}^{t_{end}} |X_{ref} - X_k|. \tag{10}$$

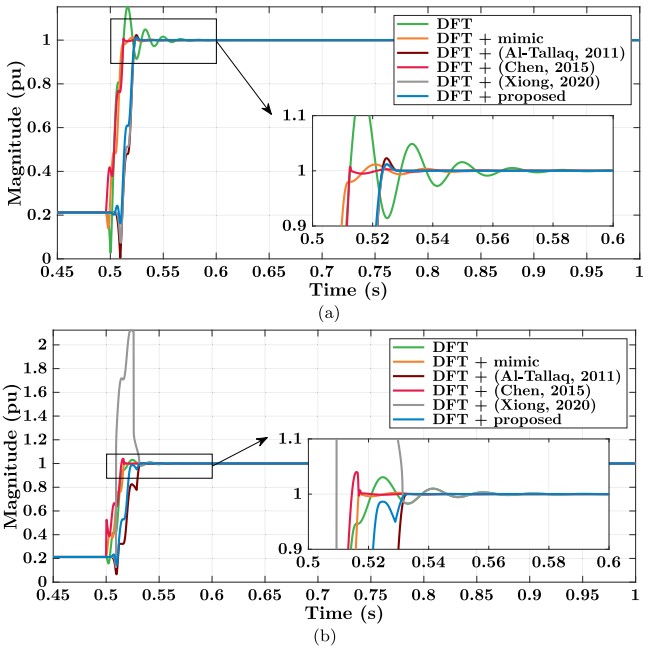

Fig. 3. The responses of all filters for a solid single-phase fault at 50 km from bus 1 and fault inception angle of (a) 0° and (b) 90°.

A low value for this index indicates few oscillations due to the EDDC component. The second performance index (PI_2) is the percentage overshoot of the phasor estimation after the fault, as presented in (11):

$$PI_2 = max(X - X_{ref}) \cdot 100. \tag{11}$$

As this overshoot is mostly caused by the EDDC component presented in the input signal, an ideal filter should have no overshoot.

Next, the phasors were estimated using the conventional DFT algorithm, considering measurements with a sampling rate of 128 samples/cycle (7680 Hz). Additionally, a second order low-pass filter with a cut-off frequency of 1 kHz was used to preprocess the input signals, as it would be present in a real implementation to prevent aliasing.

4.2. Single contingency scenario

As the approaches have different formulations, they also have distinct responses. To visualize them, the responses of each approach for a solid single-phase fault in the middle of the line are presented in Fig. 3.

The first case, illustrated in Fig. 3(a), shows that all the approaches drastically reduced the steady-state oscillations and overshoot of the reference case with no filter (in green). Nevertheless, for the second case, shown in Fig. 3(b), it was observed that some approaches' performances were deteriorated by the change in the fault inception angle. Furthermore, to allow a better visualization of the performances over certain parameters, the results were divided into multiple tables and figures. Tables 1 and 2 show the average results sorted by fault distances regarding PI_1 and PI_2, respectively. The bold values in the tables are the smallest performance indices, considering a margin of error up to 5%.

The proposed approach presented the lowest performance indices for all distances, as shown in Tables 1 and 2. Thus, it proves that the proposed approach was not influenced by the fault distance. In contrast, some approaches had divergent results in certain distances, also presenting worse performance indices than the reference case with no filter, as for the approaches proposed by [13,26]. Additionally, Tables 3 and 4 display the average values of PI_1 and PI_2, respectively, sorted by fault resistances.

Table 1
Average values of PI_1 for all faults per distance from bus 1.

Filters	1 km	10 km	20 km	30 km	40 km	50 km	60 km	70 km	80 km	90 km
No filter	5.45	5.25	6.09	6.40	6.01	5.85	5.85	6.06	6.17	6.45
Mimic filter [2]	2.00	1.61	2.33	2.55	2.10	1.92	1.93	2.16	2.34	2.71
(Al-Tallaq, 2011) [8]	1.67	1.23	1.88	2.05	1.53	1.30	1.30	1.54	**1.73**	**2.12**
(Chen, 2015) [13]	2.47	2.75	2.36	2.46	2.36	2.73	2.71	2.77	2.60	2.56
(Xiong, 2020) [26]	21.2	25.0	20.6	81.1	31.7	49.2	44.7	81.2	26.7	75.4
Proposed	**1.45**	**1.03**	**1.70**	**1.91**	**1.41**	**1.21**	**1.21**	**1.46**	**1.65**	**2.04**

Table 2
Average values of PI_2 for all faults per distance from bus 1.

Filters	1 km	10 km	20 km	30 km	40 km	50 km	60 km	70 km	80 km	90 km
No filter	7.10	7.40	7.61	7.72	7.75	7.71	7.63	7.48	7.26	6.95
Mimic filter [2]	1.32	1.33	1.35	1.35	1.35	1.35	1.35	1.36	1.38	1.41
(Al-Tallaq, 2011) [8]	1.26	1.20	1.13	1.06	0.98	0.91	0.84	0.76	0.69	0.61
(Chen, 2015) [13]	6.47	6.42	6.51	6.67	6.88	7.15	7.47	7.85	8.32	8.93
(Xiong, 2020) [26]	19.8	23.1	19.2	66.2	28.0	41.1	38.2	66.6	23.5	61.4
Proposed	**0.55**	**0.54**	**0.52**	**0.49**	**0.45**	**0.42**	**0.38**	**0.35**	**0.31**	**0.28**

Table 3
Average values of PI_1 for all faults per fault resistance.

Filters	0 Ω	2 Ω	4 Ω	6 Ω	8 Ω	10 Ω	12 Ω	14 Ω	16 Ω	18 Ω	20 Ω
No filter	10.5	9.01	8.02	7.07	6.42	5.47	4.51	3.72	4.11	3.58	3.10
Mimic filter [2]	2.05	2.09	2.34	2.40	2.59	2.31	1.90	1.59	2.37	2.18	1.98
(Al-Tallaq, 2011) [8]	**1.58**	1.47	1.68	1.76	1.97	1.75	1.38	1.11	1.93	1.77	1.57
(Chen, 2015) [13]	1.97	2.12	2.15	2.06	2.31	2.40	2.91	3.16	3.04	2.96	3.27
(Xiong, 2020) [26]	75.6	17.0	118	32.2	37.6	19.4	42.1	23.0	19.7	35.0	82.4
Proposed	**1.52**	**1.39**	**1.58**	**1.64**	**1.84**	**1.61**	**1.24**	**0.96**	**1.78**	**1.61**	**1.42**

Table 4
Average values of PI_2 for all faults per fault resistance.

Filters	0 Ω	2 Ω	4 Ω	6 Ω	8 Ω	10 Ω	12 Ω	14 Ω	16 Ω	18 Ω	20 Ω
No filter	9.57	9.87	9.64	9.11	8.42	7.67	6.90	6.18	5.50	4.88	4.32
Mimic filter [2]	0.72	1.05	1.28	1.41	1.47	1.48	1.48	1.47	1.48	1.51	1.56
(Al-Tallaq, 2011) [8]	0.83	0.87	0.91	0.95	0.99	1.00	1.01	0.98	0.97	0.94	0.91
(Chen, 2015) [13]	6.00	5.93	5.97	6.11	6.37	6.73	7.20	7.79	8.47	9.24	10.1
(Xiong, 2020) [26]	60.9	15.7	94.6	28.3	32.3	18.5	36.7	21.9	18.4	30.5	67.8
Proposed	**0.45**	**0.46**	**0.46**	**0.46**	**0.46**	**0.45**	**0.43**	**0.41**	**0.40**	**0.38**	**0.35**

As shown in Tables 3 and 4, the proposed approach presented the best performance indices. Nonetheless, the approaches proposed by [13,26] had divergences for some values of fault resistance, presenting oscillations and overshoots higher than the reference case with no filter. Moreover, Fig. 4 shows the average results sorted by fault inception angles.

The proposed approach had some of the smallest steady-state average errors (PI_1), as can been seen in Fig. 4(a). Regarding the overshoot (PI_2, shown in Fig. 4(b)), the proposed approach presented a similar performance, maintaining an overall overshoot below 1%. Despite the approach in [26] performing better than the proposed approach concerning angles under ±60°, it performed poorly for fault inception angles in a range from 60° to 120° and 250° to 300°, reaching average overshoots above 100%. Moreover, the approach proposed by [13] also presented overshoots greater than the reference case for certain inception angles. The other two approaches, [2,8], presented reasonable results for all the cases, mostly improving the response from the reference case. Finally, the average results from all simulated faults are summarized in Table 5.

Overall, the proposed approach had the best average results considering all the simulated single-phase faults. The approaches proposed by [2,8] also presented good results. Nonetheless, due to divergences in certain fault conditions, the average results from the approach proposed by [13] had smaller steady-state errors than the reference case, but they were similar regarding the overshoot. On the other hand, the overall performance of [26] was worse than the reference case, partially explained by huge divergences, even though it eventually converged to the final steady-state value.

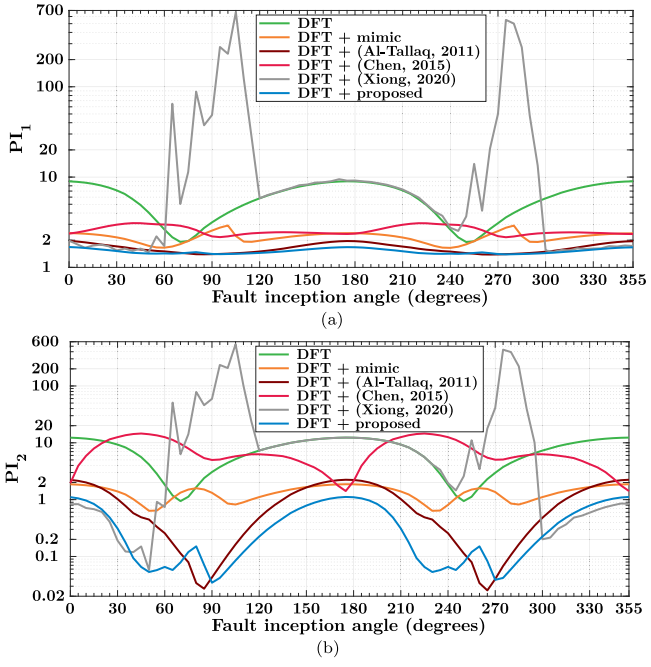

Fig. 4. Average results for all faults per inception angle for (a) PI_1 and (b) PI_2.

Table 5
Average results for all single-phase faults simulated.

Filters	PI_1	PI_2
No filter	5.958	7.46
Mimic filter [2]	2.164	1.36
(Al-Tallaq, 2011) [8]	1.634	0.94
(Chen, 2015) [13]	2.577	7.27
(Xiong, 2020) [26]	45.68	38.7
Proposed	**1.507**	**0.43**

Table 6
Harmonic currents in percentage for each harmonic profile.

Harmonic	Profile 1	Profile 2	Profile 3	Profile 4	Profile 5
3rd	1.50%	0.15%	0.00%	13.80%	1.20%
5th	22.00%	0.55%	17.00%	5.05%	33.60%
7th	15.00%	0.29%	10.10%	2.59%	1.60%
9th	0.00%	0.00%	0.00%	1.57%	0.00%
11th	10.20%	6.20%	6.10%	1.05%	8.70%
13th	8.40%	4.50%	4.42%	0.75%	1.20%
15th	0.00%	0.00%	0.00%	0.57%	0.00%
17th	4.30%	0.10%	3.83%	0.44%	4.50%
19th	3.40%	0.21%	3.20%	0.35%	1.30%
21st	0.00%	0.00%	0.00%	0.29%	0.00%
23rd	0.59%	0.46%	2.58%	0.24%	2.80%
25th	0.00%	0.00%	2.32%	0.20%	0.00%
THD	30.27%	7.70%	22.02%	15.09%	35.21%

Table 7
Average results for all faults simulated considering the presence of different harmonic profiles.

Filters	Profile 1 PI_1	Profile 2 PI_1	Profile 3 PI_1	Profile 4 PI_1	Profile 5 PI_1
No filter	5.991	5.961	5.980	5.985	5.992
Mimic filter [2]	2.201	2.168	2.183	2.178	2.190
(Al-Tallaq, 2011) [8]	1.642	1.635	1.639	1.633	1.640
(Chen, 2015) [13]	2.694	2.577	2.648	2.564	2.710
(Xiong, 2020) [26]	38.63	35.07	97.52	25.30	41.13
Proposed	**1.511**	**1.507**	**1.510**	**1.508**	**1.510**

4.3. Harmonics

As the filters should remain reliable for applications on protection, the presence of harmonics in the input signal should not influence their performances, as mentioned in [27–29]. Therefore, five harmonic profiles were used, corresponding to 6 and 12-pulse rectifiers, static frequency converters, thyristor-controlled reactors, and DC motors (as presented in [30]), which will be referred to as profiles 1 to 5, respectively. The harmonic currents and Total Harmonic Distortion (THD) in percentage for each harmonic profile are shown in Table 6.

For this analysis, the harmonic currents were injected at bus 1 using the pre-fault current magnitudes as a reference to define the magnitude of each harmonic. Then, all 7920 faults from the previous section were simulated again for each one of the harmonic profiles. The steady-state errors (PI_1) for all the approaches in this analysis are presented in Table 7.

All approaches, except Ref. [26], kept a similar steady-state error for all the harmonic profiles, which was smaller than the reference case with no filter. Additionally, the proposed approach presented the best performance of all the approaches tested.

4.4. Noise

To analyze the robustness of the approaches in noisy conditions, a white Gaussian noise was added to all current signals simulated, using different values of signal-to-noise ratios (SNRs), that were: 30 dB, 35 dB, 40 dB, 50 dB, and 60 dB. The average results for each noise level are shown in Table 8.

Table 8
Average results for all faults simulated in the presence of different noise levels.

Filters	30 dB PI_1	35 dB PI_1	40 dB PI_1	50 dB PI_1	60 dB PI_1
No filter	**32.81**	19.71	12.73	7.194	5.996
Mimic filter [2]	45.77	24.93	13.78	4.743	2.507
(Al-Tallaq, 2011) [8]	39.19	21.16	11.53	3.787	1.935
(Chen, 2015) [13]	389.3	209.5	113.0	33.55	10.75
(Xiong, 2020) [26]	251.1	95.06	56.35	34.58	44.45
Proposed	**32.60**	**17.65**	**9.655**	**3.239**	**1.748**

Table 9
Average results for different sampling rates.

Filters	64		128		256		512	
	PI_1	PI_2	PI_1	PI_2	PI_1	PI_2	PI_1	PI_2
No filter	5.050	7.50	5.958	7.46	9.884	7.45	18.74	7.45
Mimic filter [2]	3.170	1.40	2.164	1.36	2.266	1.34	3.480	1.34
(Al-Tallaq, 2011) [8]	**2.909**	0.98	1.634	0.94	1.200	0.93	1.345	0.93
(Chen, 2015) [13]	**2.937**	7.38	2.577	7.27	3.515	7.29	6.234	7.31
(Xiong, 2020) [26]	17.05	26.33	45.68	38.7	100.5	43.1	110.9	25.8
Proposed	**2.848**	**0.47**	**1.507**	**0.43**	**0.941**	**0.42**	**0.827**	**0.42**

For the cases with an SNR equal to 30 dB and 35 dB, the proposed approach was the only one to present a result better than the reference case. As the approach from [13] uses a second order derivative, the noise had a significant impact on its performance. The approach proposed by [2] also had a poor performance for noisy signals, as the digital mimic filter tends to amplify the high frequency content. When using the approach from [8], reasonable results were reached for low noise level. In contrast, the approach used by [26] had the worst performance of all the approaches tested with a low noise level.

4.5. Influence of the sampling rate

To investigate how the sampling rate affects the performance of the approaches, additional tests were carried out. Maintaining the DFT for phasor estimation, all the test signals were re-evaluated using the following sampling rates: 64, 256, and 512 samples/cycle. The final results, including the case with 128 samples/cycle (used in the previously presented tests), are illustrated in Table 9.

Due to the increase in samples, most of the errors also increased. However, the proposed approach and the approach from [8] presented a decrease in the evaluation indices, as the accuracy of the moving average and numerical integration increases with a higher number of samples. To summarize, the proposed approach proved to perform better than the other approaches, disregarding the sampling rate utilized.

4.6. Frequency response

As electrical power system frequency might vary around its nominal value, the frequency response of the approaches had to be analyzed. For this investigation, the approaches were evaluated considering their combined frequency response with the DFT. Fig. 5 shows the frequency response for each method.

As illustrated in Fig. 5, some approaches behaved similarly to the DFT, presenting a constant reduction in the gain as the frequency increased. Nonetheless, the approach proposed by [13] increased its gain up to 900 Hz and then started decreasing. On the other hand, the approach proposed by [26] presented an oscillatory response, sometimes reaching a gain close to 700 pu. Despite this, all approaches had a unit gain at 60 Hz.

As defined in the IEEE Standard 1547-2018, all generators must operate in a range of frequency between 58.5 Hz and 61.2 Hz [31]. Except for the approach proposed by [26], the approaches maintained a gain close to 1 within this range. Table 10 shows the maximum gain

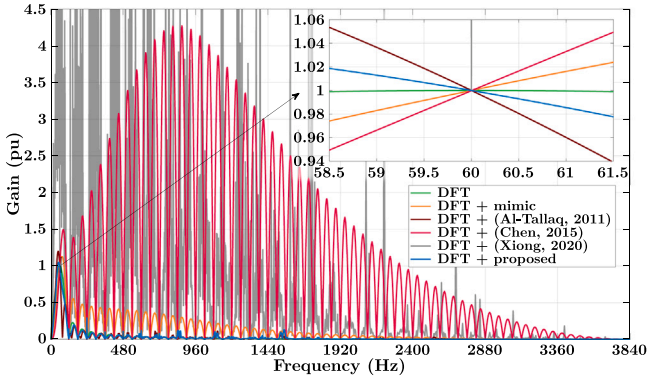

Fig. 5. The combined frequency responses of all filters with the DFT.

Table 10
Maximum gain variation between 58.5 Hz and 61.2 Hz.

Filters	Gain variation
No filter	0.0010
Proposed	0.0362
Mimic filter [2]	0.0450
(Chen, 2015) [13]	0.0900
(Al-Tallaq, 2011) [8]	0.1015
(Xiong, 2020) [26]	213.99

variation in the range of 58.5 Hz and 61.2 Hz defined by the IEEE standard. This variation was computed from the difference between the maximum and minimum gain within the specified range.

The proposed approach had the lowest variation when analyzing the response for all the approaches, and the approach proposed by [26] had the highest one. Furthermore, as the frequency response is an intrinsic characteristic of a filter, the magnitude of the input signal can be corrected when the current frequency is known, thus minimizing the effect of frequency variation on its response.

4.7. Tests in hardware

To better analyze the performance of the approaches, they were embedded in hardware. The laboratory setup for the tests is shown in Fig. 6. The setup uses the oscilloscope and arbitrary waveform generator Analog Discovery 2 from Digilent. Additionally, an active second order low-pass filter with a cut-off frequency of 1 kHz was used to further mitigate noise. The approaches were embedded in microcontroller F28379D from Texas Instruments, which has a 32-bit dual core ARM chip at 200 MHz. The DFT was kept as the phasor estimation algorithm, with a sampling rate of 128 samples per cycle (7680 Hz) and a reporting rate of 8 phasors per cycle (480 Hz).

Utilizing the arbitrary waveform generator, the fault signals simulated in the ATP software were generated at 512 samples/cycle (30,720 Hz) and read by the microcontroller, with a sampling rate of 128 samples per cycle. Nevertheless, for this analysis, the number of fault cases was reduced to faults in the middle of the line, with three fault resistances (0, 10, and 20 Ω) and eight fault inception angles (0°, 45°, 90°, 135°, 180°, 225°, 270°, 315°). Thus, it resulted in a total of 24 faults.

In these tests, noises and digitization errors from the analog-to-digital conversion might affect the performances of the approaches, as these disturbances can insert additional DC offset in the input signal. Thus, to illustrate the oscillations in this analysis, the outputs of each approach for a solid single-phase fault in the middle of the line with fault inception angles of 0 and 90 degrees are presented in Fig. 7. Note that these are the same cases from Fig. 3. Thus, ideally the approaches should have similar responses.

Table 11
Average results for the approaches embedded in hardware.

Filters	PI_1	PI_2
No filter	11.24	7.10
Mimic filter [2]	11.46	5.03
(Al-Tallaq, 2011) [8]	11.56	7.24
(Chen, 2015) [13]	53.52	35.75
(Xiong, 2020) [26]	74.87	80.99
Proposed	**6.96**	**2.22**

Table 12
Average execution time for the approaches embedded in hardware.

Filters	Execution time	Percentage of the sampling period
Mimic filter [2]	65.77 ns	0.05%
(Xiong, 2020) [26]	146.0 ns	0.11%
(Al-Tallaq, 2011) [8]	1.965 μs	1.51%
(Chen, 2015) [13]	4.376 μs	3.36%
Proposed	4.687 μs	3.60%

Oscillations were observed for most approaches, especially for the approach proposed by [13], which was based on the second derivative of the signal. Furthermore, the approach of [26] continued to have numerical divergence problems for faults with a fault inception angle of 90 degrees, as it did for the previous tests in the simulation. The final average results for the approaches in this analysis are presented in Table 11.

As can be seen from the values in Table 11, the approaches proposed by [8,13,26] performed worse than the reference case with no filter. The digital mimic filter reduced the overshoot, but its steady-state error was slightly above the reference case. Only the proposed approach was able to mitigate the effects of the EDDC component for both indices.

4.8. Execution time comparison

Additionally to the hardware evaluation, the execution times of the algorithms were measured. The measurement was made using a digital output pin of the microcontroller. This output was set to high at the start of the EDDC filter calculation and toggled to low at the end. This procedure was executed for each embedded algorithm to ensure a fair comparison among them. Table 12 presents the average execution time for each approach after 30,000 cycles, using a sampling rate of 128 samples per cycle (7,680 Hz).

As shown in Table 12, the mimic filter was the fastest method, followed by the approaches of [8,13,26], and the approach proposed in this paper. As a reference for the execution time, the full-cycle DFT with 128 samples, also embedded in the same hardware, took 15.51 μs to run, and the sampling period for these tests was 130.21 μs. The proposed approach had an execution time similar to [13], and it was relatively close to the execution time of the other approaches. Moreover, the proposed approach was compatible with hardware-embedded applications in a low-cost microcontroller, and it did not require any type of parallel processing. Furthermore, considering the analog to digital converter conversion time, DFT algorithm execution time, and other communication delays, around 100 μs still remained between every sample to execute the mitigating algorithms. Thus, all the approaches were embedded in hardware and some processing time was still available, showing their applicability in practice.

5. Conclusions

This paper presented an alternative approach to mitigate the EDDC component in faulty transmission systems. The proposed approach used the moving average and symmetry of the signal to estimate the EDDC component, thus filtering the signal. The methodology was thoroughly evaluated with simulated signals considering real harmonic profiles,

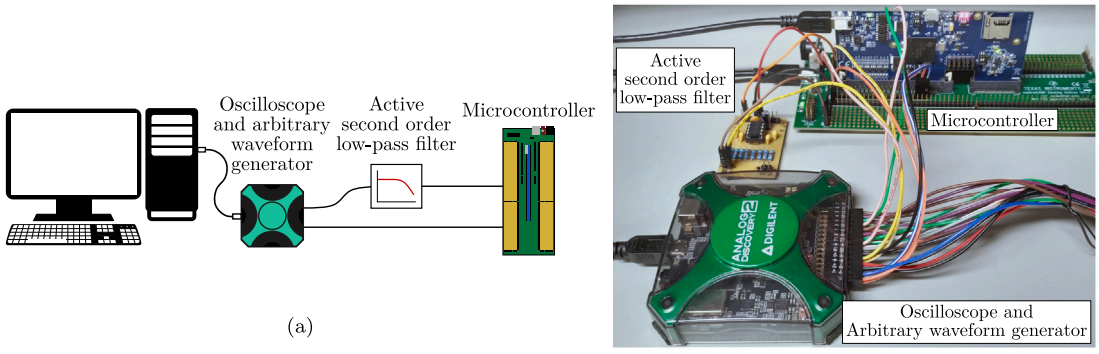

Fig. 6. Laboratory setup for the test in hardware showing the (a) connection diagram, and (b) the actual connection of the devices.

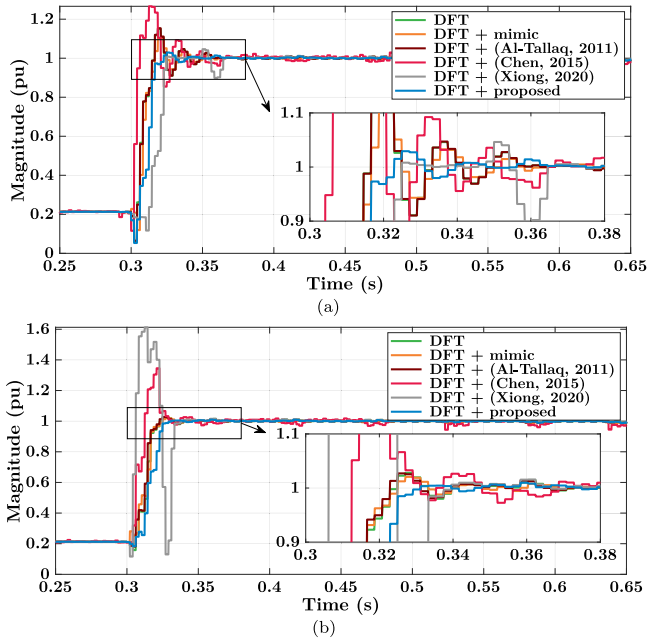

Fig. 7. The output of all filters embedded in hardware for a solid single-phase fault at 50 km from bus 1 and inception angle of (a) 0° and (b) 90°.

different noise levels, and changes in the sample rate. The results showed that the proposed approach drastically reduced the influence of the EDDC component on phasor estimation. When compared with other approaches from the literature that have a similar design, the proposed approach had a superior performance.

Additionally, the proposed approach was embedded in hardware to validate the applicability of the proposition. The proposed approach presented an execution time compatible with hardware embedded applications in a low-cost microcontroller, with no need for parallel optimizations.

Moreover, all the analysis considered numerical indices to quantify the software performance of each approach analyzed. The proposed approach presented the best results in all tests. Furthermore, as the proposed approach is a filtering technique, it can be widely applied with any phasor estimation technique to improve its performance in the presence of EDDC components.

CRediT authorship contribution statement

T.S. Menezes: Conceptualization, Methodology, Software, Validation, Formal Analysis, Data curation, Writing – original draft, Writing – review & editing, Visualization. **R.A.S. Fernandes:** Conceptualization, Writing – review & editing. **D.V. Coury:** Conceptualization, Writing – review & editing, Resources, Supervision, Project administration, Funding acquisition.

Declaration of competing interest

The authors declare that they have no known competing financial interests or personal relationships that could have appeared to influence the work reported in this paper.

Data availability

Data will be made available on request.

Acknowledgments

This work was supported in part by the São Paulo Research Foundation (FAPESP), Brazil [Grant Number 2017/16742-7 and 2021/04872-9] and Coordenação de Aperfeiçoamento de Pessoal de Nível Superior – Brazil (CAPES) [Finance Code 001].

References

[1] E. Schweitzer, D. Hou, Filtering for protective relays, in: IEEE WESCANEX 93 Communications, Computers and Power in the Modern Environment - Conference Proceedings, 1993, pp. 15–23, http://dx.doi.org/10.1109/WESCAN.1993.270548.

[2] G. Benmouyal, Removal of DC-offset in current waveforms using digital mimic filtering, IEEE Trans. Power Deliv. 10 (2) (1995) 621–630, http://dx.doi.org/10.1109/61.400869.

[3] E. Rosolowski, J. Izykowski, B. Kasztenny, A new half-cycle adaptive phasor estimator immune to the decaying DC component for digital protective relaying, in: 32nd Annual North American Power Symposium 2000, Waterloo, Canada, 2000, pp. 23–24.

[4] D.G. Hart, D. Novosel, R.A. Smith, Modified cosine filters, 2000, US Patent 6,154,687.

[5] Y. Guo, M. Kezunovic, D. Chen, Simplified algorithms for removal of the effect of exponentially decaying DC-offset on the Fourier algorithm, IEEE Trans. Power Deliv. 18 (3) (2003) 711–717, http://dx.doi.org/10.1109/TPWRD.2003.813894.

[6] M.R. Dadash Zadeh, Z. Zhang, A new DFT-based current phasor estimation for numerical protective relaying, IEEE Trans. Power Deliv. 28 (4) (2013) 2172–2179, http://dx.doi.org/10.1109/TPWRD.2013.2266513.

[7] A. Rahmati, R. Adhami, An effective filtering algorithm to mitigate transient decaying DC offset, Proc. IEEE Power Eng. Soci. Transm. Distribu. Conf. 29 (2) (2014) 966–968, http://dx.doi.org/10.1109/tdc.2014.6863450.

[8] K.N. Al-Tallaq, H.D. Al-Sharai, M.E. El-Hawary, Online algorithm for removal of decaying DC-offset from fault currents, Electr. Power Syst. Res. 81 (7) (2011) 1627–1629, http://dx.doi.org/10.1016/j.epsr.2011.03.019.

[9] A.A. Abdoos, S.A. Gholamian, M. Farzinfar, Accurate and fast DC offset removal method for digital relaying schemes, IET Gener. Transm. Distrib. 10 (8) (2016) 1769–1777, http://dx.doi.org/10.1049/iet-gtd.2014.1150.

[10] M. Tajdinian, A.R. Seifi, M. Allahbakhshi, Half-cycle method for exponentially DC components elimination applicable in phasor estimation, IET Sci. Meas. Technol. 11 (8) (2017) 1032–1042, http://dx.doi.org/10.1049/iet-smt.2017.0028.

[11] Z. Jiang, S. Miao, P. Liu, A modified empirical mode decomposition filtering-based adaptive phasor estimation algorithm for removal of exponentially decaying DC offset, IEEE Trans. Power Deliv. 29 (3) (2014) 1326–1334, http://dx.doi.org/10.1109/TPWRD.2014.2299808.

[12] M. Tajdinian, M.Z. Jahromi, K. Mohseni, S.M. Kouhsari, An analytical approach for removal of decaying DC component considering frequency deviation, Electr. Power Syst. Res. 130 (2016) 208–219, http://dx.doi.org/10.1016/j.epsr.2015.09.007.

[13] Y. Chen, T. Ji, Q. Wu, M. Li, Exponentially decaying DC offset removal for phasor measurement using second-order differential, IEEJ Trans. Electr. Electron. Eng. 10 (6) (2015) 726–728, http://dx.doi.org/10.1002/tee.22153.

[14] C.D. da Silva, G.C. Junior, L. Mariotto, G. Marchesan, Phasor estimation in power systems using a neural network with online training for numerical relays purposes, IET Sci. Meas. Technol. 9 (7) (2015) 836–841, http://dx.doi.org/10.1049/iet-smt.2014.0312.

[15] Kim, Sok, Kang, Lee, Nam, A study on deep neural network-based DC offset removal for phase estimation in power systems, Energies 12 (9) (2019) 1619, http://dx.doi.org/10.3390/en12091619.

[16] L. Wang, J. Suonan, A fast algorithm to estimate phasor in power systems, IEEE Trans. Power Deliv. 32 (3) (2017) 1147–1156, http://dx.doi.org/10.1109/TPWRD.2014.2342242.

[17] K. Chauhan, M.V. Reddy, R. Sodhi, A novel distribution-level phasor estimation algorithm using empirical wavelet transform, IEEE Trans. Ind. Electron. 65 (10) (2018) 7984–7995, http://dx.doi.org/10.1109/TIE.2018.2801837.

[18] B. Jafarpisheh, S.M. Madani, F. Parvaresh, Phasor estimation algorithm based on complex frequency filters for digital relaying, IEEE Trans. Instrum. Meas. 67 (3) (2018) 582–592, http://dx.doi.org/10.1109/TIM.2017.2783099.

[19] J.K. Hwang, C.K. Song, M.G. Jeong, DFT-Based phasor estimation for removal of the effect of multiple DC components, IEEE Trans. Power Deliv. 33 (6) (2018) 2901–2909, http://dx.doi.org/10.1109/TPWRD.2018.2825257.

[20] K.W. Min, S. Santoso, DC offset removal algorithm for improving location estimates of momentary faults, IEEE Trans. Smart Grid 9 (6) (2018) 5503–5511, http://dx.doi.org/10.1109/TSG.2017.2688981.

[21] M. Pazoki, A new DC-offset removal method for distance-relaying application using intrinsic time-scale decomposition, IEEE Trans. Power Deliv. 33 (2) (2018) 971–980, http://dx.doi.org/10.1109/TPWRD.2017.2728188.

[22] B. Jafarpisheh, S.M. Madani, S. Jafarpisheh, Improved DFT-Based phasor estimation algorithm using down-sampling, IEEE Trans. Power Deliv. 33 (6) (2018) 3242–3245, http://dx.doi.org/10.1109/TPWRD.2018.2831005.

[23] B.R. Kumar, A. Kumar, Mitigation of the DC offset by a sub-cycle sample method M-class PMUs, IEEE Trans. Power Deliv. 34 (2) (2019) 780–783, http://dx.doi.org/10.1109/TPWRD.2019.2892600.

[24] R. Godse, S. Bhat, Real-time digital filtering algorithm for elimination of the decaying DC component using mathematical morphology, IET Gener. Transm. Distrib. 13 (15) (2019) 3230–3239, http://dx.doi.org/10.1049/iet-gtd.2018.5476.

[25] W.J. Kim, S.R. Nam, S.H. Kang, Adaptive phasor estimation algorithm based on a least squares method, Energies 12 (7) (2019) http://dx.doi.org/10.3390/en12071387.

[26] L. Xiong, X. Liu, C. Zhao, F. Zhuo, A fast and robust real-time detection algorithm of decaying dc transient and harmonic components in three-phase systems, IEEE Trans. Power Electron. 35 (4) (2020) 3332–3336, http://dx.doi.org/10.1109/TPEL.2019.2940891.

[27] J. Fuller, E. Fuchs, D. Roesler, Influence of harmonics on power distribution system protection, IEEE Trans. Power Deliv. 3 (2) (1988) 549–557, http://dx.doi.org/10.1109/61.4292.

[28] W. Elmore, C. Kramer, S. Zocholl, Effect of waveform distortion on protective relays, IEEE Trans. Ind. Appl. 29 (2) (1993) 404–411, http://dx.doi.org/10.1109/28.216551.

[29] J. Jedrzejczak, G.J. Anders, M. Fotuhi-Firuzabad, H. Farzin, F. Aminifar, Reliability assessment of protective relays in harmonic-polluted power systems, IEEE Trans. Power Deliv. 32 (1) (2017) 556–564, http://dx.doi.org/10.1109/TPWRD.2016.2544801.

[30] C.-H. Lin, C.-H. Wang, Adaptive wavelet networks for power-quality detection and discrimination in a power system, IEEE Trans. Power Deliv. 21 (3) (2006) 1106–1113, http://dx.doi.org/10.1109/TPWRD.2006.874105.

[31] IEEE Standard for Interconnection and Interoperability of Distributed Energy Resources with Associated Electric Power Systems Interfaces, IEEE Std 1547-2018 (Revision of IEEE Std 1547-2003), 2018, pp. 1–138, http://dx.doi.org/10.1109/IEEESTD.2018.8332112.